

Physical properties of near-Earth Asteroid (33342) 1998 WT24

Michael W. Busch^{a,*}, Lance A.M. Benner^b, Steven J. Ostro^b, Jon D. Giorgini^b,
Raymond F. Jurgens^b, Randy Rose^b, Daniel J. Scheeres^c, Christopher Magri^d, Jean-Luc Margot^e,
Michael C. Nolan^f, Alice A. Hine^f

^a Division of Geological and Planetary Sciences, California Institute of Technology, MC 150-21, Pasadena, CA 91125, USA

^b Jet Propulsion Laboratory, California Institute of Technology, Pasadena, CA 91109, USA

^c Department of Aerospace Engineering, University of Michigan, 1320 Beal Avenue, Ann Arbor, MI 48109, USA

^d University of Maine at Farmington, Preble Hall, 173 High St., Farmington, ME 04938, USA

^e Department of Astronomy, Cornell University, 304 Space Sciences Bldg., Ithaca, NY 14853, USA

^f Arecibo Observatory, National Astronomy and Ionosphere Center, Box 995, Arecibo, PR 00613, USA

Received 5 November 2007; revised 29 January 2008

Available online 29 February 2008

Abstract

During its close Earth approach in 2001, the E-class near-Earth Asteroid (33342) 1998 WT24 was the focus of extensive radar, optical, and thermal infrared observations. We present a physical model of this object, estimated from Arecibo and Goldstone radar images that cover multiple rotations and span over 100° of sky motion. The asteroid has an equivalent diameter of 415 ± 40 m and a diffuse radar scattering law that is identical in both senses of circular polarization, implying a surface that is extremely rough on centimeter-to-decimeter scales. The shape is dominated by three large basins, which may be impact craters or a relic of past dynamical disruption of the object. Analysis of YORP perturbations on WT24's spin state predicts that the asteroid's spin rate is decreasing at a rate of $2 \times 10^{-7} \text{ deg s}^{-1} \text{ yr}^{-1}$. Simply extrapolating this rate suggests that the asteroid will despin over the next 150 kyr and was spinning at its surface disruption rate 75 kyr ago, but the rotational evolution of WT24 depends on the surface's thermal properties and probably is more complex than a simple spin-down.

© 2008 Elsevier Inc. All rights reserved.

Keywords: Asteroids, composition; Asteroids, dynamics

1. Discovery and observation history

The Earth/Venus/Mercury-crossing Asteroid (33342) 1998 WT24 (hereafter WT24) was discovered by LINEAR on 1998 December 4 (MPEC 1998-X10). It has semi-major axis 0.718 AU, eccentricity 0.418, inclination 7.34° and is near a 2:5 resonance with Mercury, a 1:1 resonance with Venus, and a 5:3 resonance with Earth. WT24 currently makes close approaches to all three planets. It also has a very low flyby Δv (velocity change from low Earth orbit to a flyby trajectory), potentially making it an appealing target for examination by a spacecraft, although the Δv for rendezvous is high.

During its close Earth approach in December 2001, WT24 was observed extensively using thermal infrared radiometry (Harris et al., 2007), optical photometry and spectroscopy (Table 1), and radar. Optical observations gave the rotation period, 3.697 ± 0.001 h (Krugly et al., 2002), and showed that WT24 is of spectral class E (Lazzarin et al., 2004). The approach, within 0.0125 AU (4.9 lunar distances), yielded radar echoes with SNRs measured in the tens of thousands for a single transmit-receive cycle. Our radar observations used many different stations: delay-Doppler imaging using Goldstone and Arecibo, as well as continuous-wave (CW) Doppler-resolved echoes received at several additional stations, including Medecina (Di Martino et al., 2004). Here we report the results of our Goldstone and Arecibo observations (Table 2).

* Corresponding author.

E-mail address: busch@caltech.edu (M.W. Busch).

2. Polarization ratio and E-class classification

In radar astronomical observations, we transmit a circularly polarized signal and then receive echoes in both senses of circular polarizations. If the asteroid's echo came entirely from single scattering, then it would be entirely in the opposite-sense-as-transmitted circular polarization (OC). A real object can have near-surface roughness on the scale of the wavelength or multiple scattering, leading to some echo power coming back in the same-sense-as-transmitted polarization (SC). The target's SC/OC ratio of echo power is a convenient measure of the degree of near-surface structural complexity.

WT24 has one of the highest polarization ratios ever recorded for an asteroid: $SC/OC = 0.97 \pm 0.10$ at the 13 cm wavelength of the Arecibo radar, over multiple rotations and days of observation, with a similarly high ratio at the 3.5 cm wavelength used at Goldstone. At Goldstone, we transmitted both senses of circular polarization as a check against instrument problems (Fig. 1, supplementary Fig. 1, supplementary Table 1). The high ratio implies extreme near-surface structural complexity. There are only 14 near-Earth asteroids with $SC/OC > 0.8$, out of 179 observed (Benner et al., 2008). These

high polarization objects include all five radar-observed near-Earth asteroids known to belong to spectral class E (presumed

Table 1
Results of optical and thermal infrared measurements

Spectral class	E (Kiselev et al., 2002; Lazzarin et al., 2004)
Rotation period	3.697 ± 0.001 h (Krugly et al., 2002; Pravec, 2007)
Harris et al. (2007)	
Effective diameter	0.35 ± 0.04 km
Optical albedo	0.56 ± 0.2
Thermal inertia	$100\text{--}300 \text{ J m}^{-2} \text{ s}^{-0.5} \text{ K}^{-1}$
Pole direction	$(\lambda, \beta) = (355^\circ, -52^\circ) \pm \sim 30^\circ$

Note. Summary of previous optical and thermal infrared measurements of WT24.

Table 2
WT24 radar observations used in shape modeling

Time	Range	(UTC)	Observatory		Resolution $\mu\text{s} \times \text{Hz}$	Sub-lat ($^\circ$)	Sky RA	Pos DEC ($^\circ$)	RTT (s)
2001	Dec 14	06:35:54–07:28:55	Goldstone	R	0.25×1.0	–5	99	29	15
2001	Dec 14	08:17:10–08:31:00	Goldstone	bR	0.125×0.5	–5	99	29	15
2001	Dec 14	12:46:50–14:05:20	Goldstone	bR	0.125×0.5	–5	99	29	15
2001	Dec 15	04:43:29–13:05:10	Goldstone	bL	0.125×0.5	–15	82	36	13
2001	Dec 16	01:37:42–05:00:02	Goldstone	bL	0.125×0.5	–24	60	41	12
2001	Dec 16	09:17:43–11:10:15	Goldstone	L	0.125×0.5	–28	51	42	12
2001	Dec 17	02:03:20–09:00:00	Goldstone	bL	0.125×0.25	–35	28	41	13
2001	Dec 18	01:32:05–07:30:24	Goldstone	bL	0.125×0.25	–38	10	36	15
2001	Dec 18	21:08:49–	Goldstone	bL	0.125×0.25	–39	358	31	19
2001	Dec 19	–06:40:31							
2001	Dec 15	04:09:08–05:17:53	Arecibo	L	0.100×0.06	–15	82	36	13
2001	Dec 17	23:03:21–	Arecibo	L	0.050×0.09	–38	11	37	15
2001	Dec 18	–00:00:42							
2001	Dec 18	22:54:05–23:03:53	Arecibo	L	0.050×0.07	–39	358	31	19
2001	Dec 19	21:22:17–23:04:40	Arecibo	L	0.100×0.06	–38	350	27	19
2001	Dec 20	20:12:52–22:28:44	Arecibo	L	0.100×0.05	–38	345	23	22

Note. Radar observations of WT24 used in shape modeling. Sub-lat is the latitude of the sub-radar point at the mid-point of the observations. Similarly, the asteroid's sky position and round-trip travel time (RTT) are given at the mid-point of each track. All the Goldstone tracks span at least one complete rotation and the last crosses a day boundary. 'b' denotes bistatic Goldstone observations, transmitting from the DSS-14 antenna at Goldstone and receiving at the nearby DSS-13 antenna to permit good frequency resolution while the asteroid was at closest approach. 'R' and 'L' denote the right and left senses of circular polarization transmitted. For a log of all observations, see supplementary Table 1.

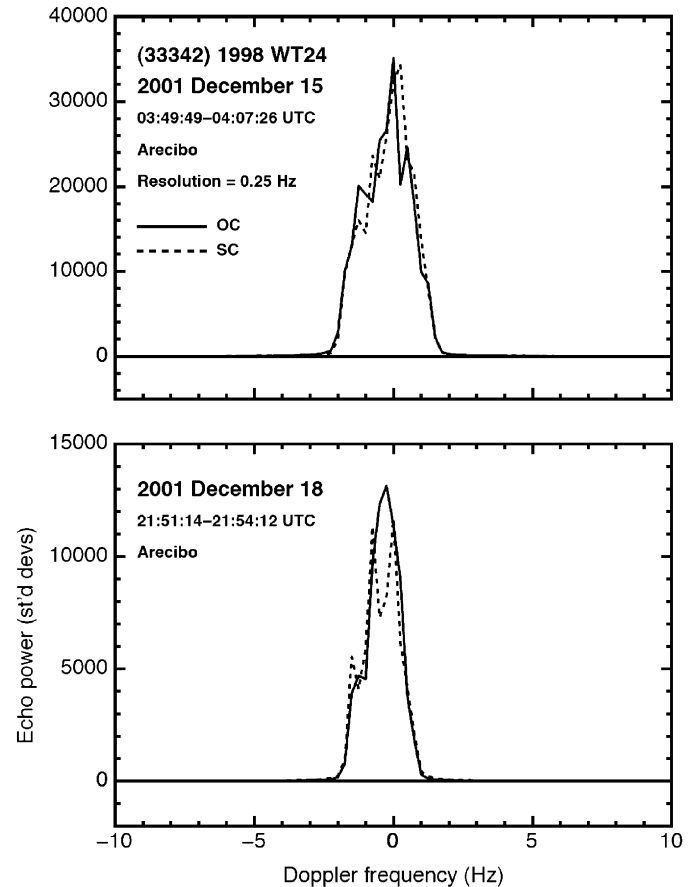


Fig. 1. Arecibo Doppler echo spectrum of WT24, normalized to the noise background, illustrating the high SC/OC polarization ratio. For a collage showing echo spectra spanning a full rotation, see supplementary Fig. 1.

to have enstatite achondrite compositions; Bus et al., 2002), including WT24, and others of unknown composition (X-class or no spectral data available).

3. Radar scattering law and shape

The delay–Doppler images of WT24 show considerable structure, identical in both polarizations (Figs. 2 and 3, supplementary Fig. 2, and supplementary movie). In particular, a large radar-dark feature we interpret as a concavity and an associated ridge-like feature are visible at one set of rotation phases and a small but conspicuous group of radar-bright pixels we interpret as a raised feature is evident beyond the leading edge of the echo. The echo has a delay depth of $\sim 1.5 \mu\text{s}$, suggesting a diameter of a few hundred meters. The echo bandwidth is roughly

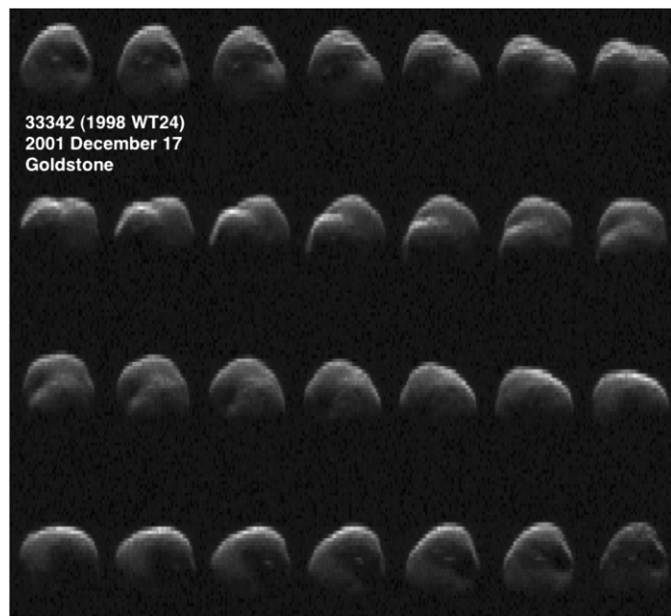


Fig. 2. Goldstone images from 2001 December 17 05:07:10–09:00:00 UTC. This collage shows one complete rotation. Time increases from left to right and top to bottom. Within each image, range from Earth increases from top to bottom and Doppler frequency from left to right. Resolution is $0.125 \mu\text{s} \times 0.5 \text{ Hz}$.

constant (varying by no more than 15%), suggesting that the asteroid is not very elongated.

We used our SHAPE software to construct a model of WT24 from the delay–Doppler images. SHAPE, described most recently by Magri et al. (2007), uses constrained weighted least-squares to estimate parameters describing the shape of the object, its rotation state, its radar scattering properties, and corrections to the delay–Doppler trajectory prediction. Because of the large volume of the WT24 dataset (totaling ~ 875 images when the data are split in time to avoid rotation smearing), we selected 99 images for use in the original fitting (Fig. 4, Table 2), chosen to cover as many orientations of the object as possible, and included all of the images only in the final iterations (supplementary Fig. 2).

The early stages of our modeling included a grid search over the entire sky with a resolution of 15° , stepping down to 3° around candidate poles. The asteroid’s motion across 110° of sky during our observations led to a well-constrained pole direction. Our pole solution, $(15^\circ, -22^\circ) \pm 5^\circ$, differs by 34° from the $(355^\circ, -52^\circ) \pm 30^\circ$ inferred by Harris et al. (2007) from thermal infrared observations.

Progressing from an ellipsoid to a spherical harmonic representation and ultimately to a 4000-vertex polyhedron, we arrived at a unique model that fit the OC images. We then took this shape model and fit it to the SC images, adjusting only the radar scattering law. The model fits the SC images as well as it fits the OC images (SC fits are shown in supplementary Fig. 3), with an indistinguishable scattering law. The polarization of the echo from WT24 is essentially randomized, and the scattering is completely diffuse, only slightly different from a Lambertian surface. We did not fit the asteroid’s shape to the lightcurve data of Krugly et al. (2002) or Pravec (2007), because those data were not presented with the times of individual lightcurve points, but our shape model qualitatively matches the structure of the lightcurve with an optical scattering law that contains minimal limb darkening.

There is some subtle structure in the images that our model does not fit, particularly near the low- and high-Doppler limits of the echo. At some level, our scattering law assumptions are simplistic: one scattering law will not hold over the en-

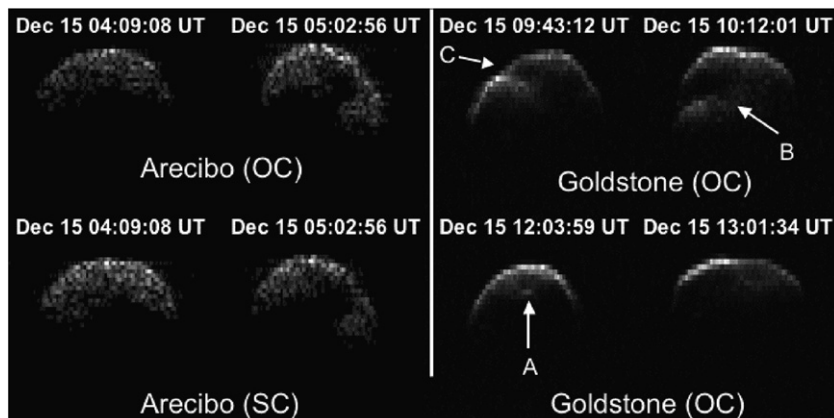


Fig. 3. Collage of selected radar images of WT24, showing surface features and the similarity between SC and OC images. Note the structure behind the leading edge (A, B), as well as the structure of the edge itself (C). The small feature A is also visible in Fig. 2.

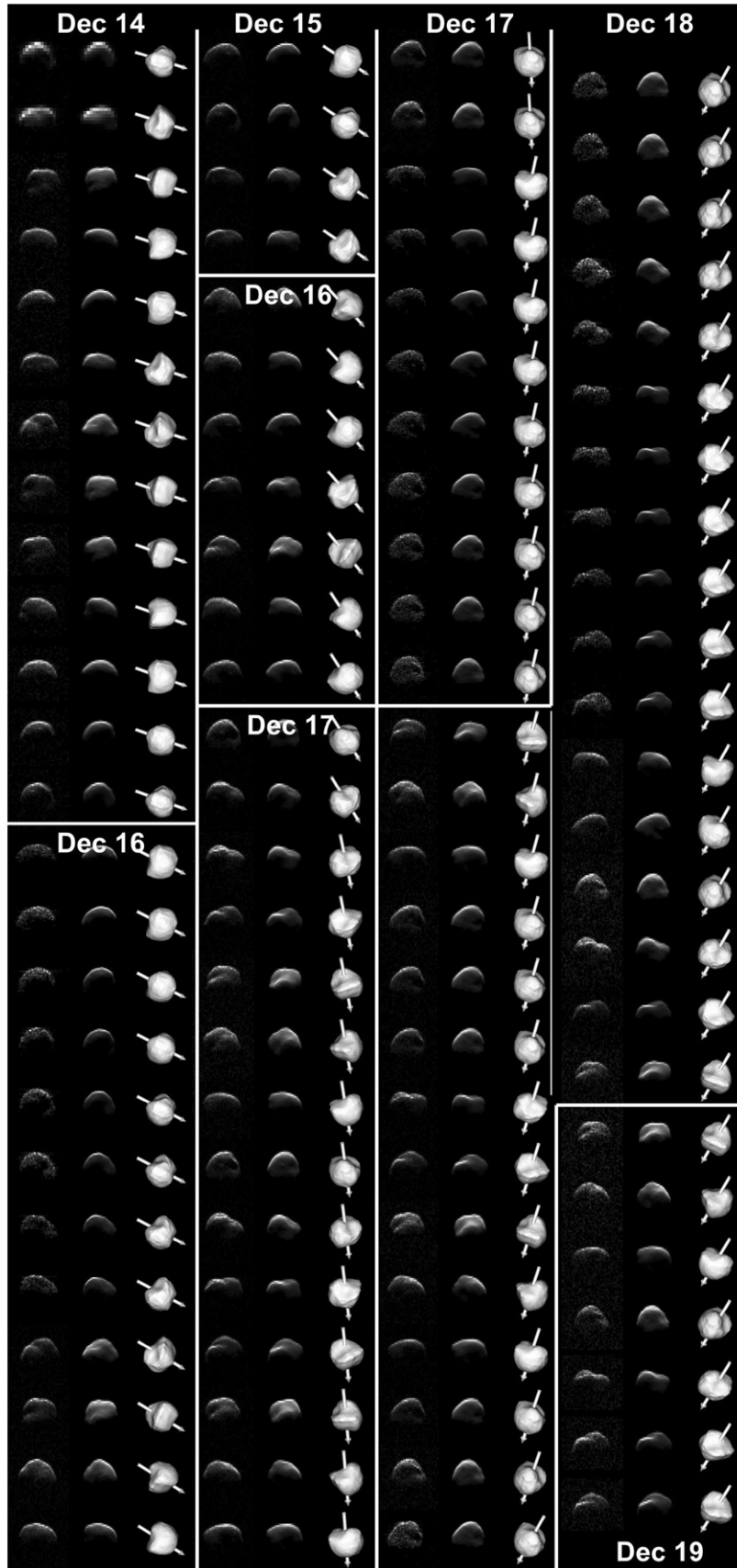


Fig. 4. Collage showing decimated radar image dataset (99 OC images), corresponding model fits, and plane-of-sky views of the model. Time increases from top to bottom and left to right. This is $\sim 1/10$ of the full dataset. The complete dataset used in shape modeling is given in supplementary Fig. 3.

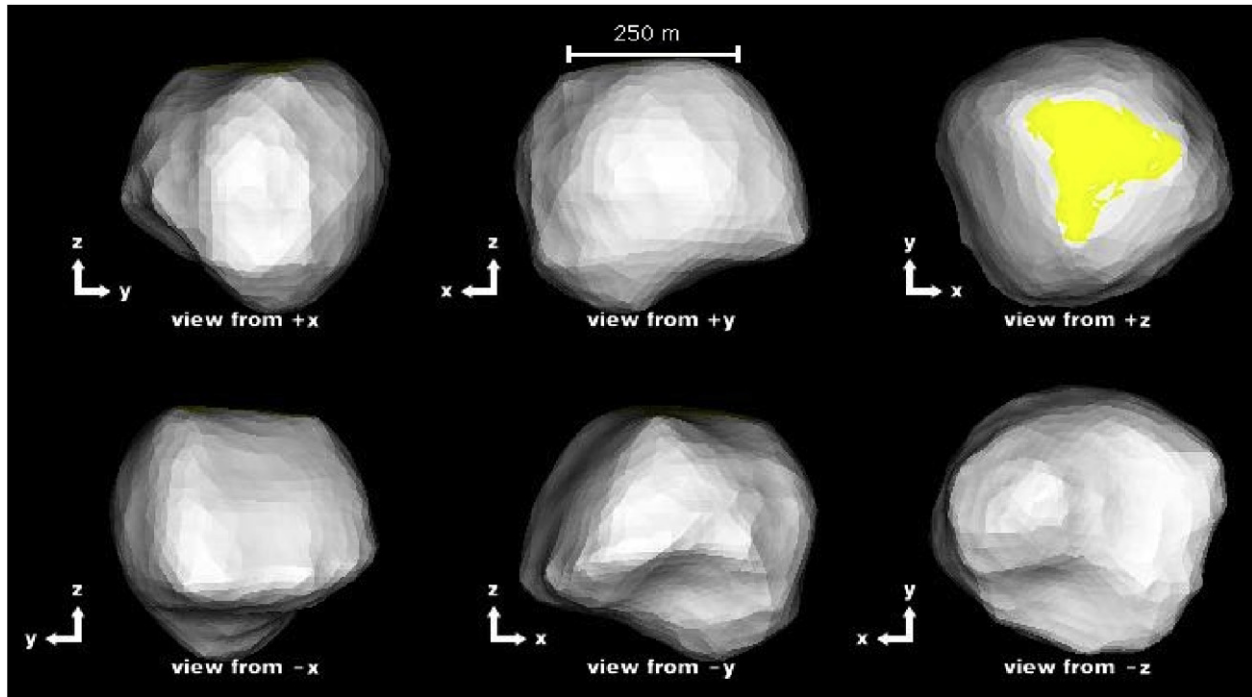


Fig. 5. Principal-axis projections of the WT24 model. The yellow shading denotes regions of the object that were never seen at incidence angles $<75^\circ$.

tire surface and a simple cosine law will not be exactly correct everywhere. This makes fitting the extremes of the echo somewhat problematic, and may be reflected in facet-scale errors in the model.

Our model's principal-axis extents are $(470 \times 425 \times 400) \pm 40$ m (Table 2), where the uncertainty is dominated by our Doppler resolution. The shape is dominated by three concavities, comparable in size to the extent of the object (Fig. 5), reminiscent of the impact craters seen on 433 Eros (Veverka et al., 2000) and 253 Mathilde (Veverka et al., 1999) although much smaller in scale. The small bright feature we observed behind the leading edge in the images is the ridge between the two basins near the south pole.

Given the model's dimensions and the estimates of the asteroid's radar cross-section (Table 3) and absolute magnitude H , we can estimate its radar and optical albedos (radar albedo = radar cross-section/cross-sectional area; optical albedo = $10^{-0.4H}$ (1329 km/effective diameter) 2 ; Pravec and Harris, 2007). WT24's total-power (SC + OC) radar albedo, 0.42, is towards the high end of the distribution of asteroid radar targets (Benner, 2008).

No high-accuracy absolute magnitude is available for WT24. The values reported from astrometric observations, and included, e.g., in the JPL Horizons database, have a spread of over a full magnitude and are systematically non-physically high. While Kiselev et al. (2002) claim a zero-phase-angle V-band magnitude of 18.69 ± 0.08 from their photometric measurements, this value may be offset from the true absolute magnitude because of opposition surge effects. We therefore consider WT24's absolute magnitude to be uncertain by ~ 0.3 mag, the largest E-type opposition surge amplitude (Belskaya et al., 2003). Taking $H = 18.69 \pm 0.3$, WT24 has a very high optical

Table 3
Properties of WT24 shape model

Principal-axis dimensions	$(470 \times 425 \times 400) \pm 40$ m
DEEVE dimensions	$(454 \times 417 \times 378) \pm 40$ m
Equivalent diameter	415 ± 40 m
Surface area	0.57 ± 0.12 km 2
Volume	0.038 ± 0.01 km 3
Rotation period	3.6970 ± 0.0002 h
Pole direction, J2000 ecliptic	$(15^\circ, -22^\circ) \pm 5^\circ$
Radar scattering law index	
OC:	
C:	0.81 ± 0.05
SC:	
C:	0.84 ± 0.05
Mean gravitational slope	11.6°
Maximum gravitational slope	40°
Range in potential across surface	0.14 m s $^{-1}$.
Mean radar cross-section	0.027 ± 0.003 km 2 (S-band, 13-cm)
Total power (SC + OC) radar albedo	0.42 ± 0.04
Optical albedo	0.34 ± 0.20

Note. DEEVE = dynamically-equivalent equal-volume ellipsoid, an ellipsoid with the same volume and principal moments of inertia as our model. Gravitational slopes and potential range assume a uniform bulk density of 3 g cm $^{-3}$. Radar scattering law index C is such that the radar cross-section/surface area $\propto \cos(\text{scattering angle})^{2C}$. A Lambertian surface would have $C = 1$.

albedo for an asteroid: 0.34 ± 0.2 [for comparison, Harris et al. (2007) obtained 0.56 ± 0.2], corresponding to the reflectances of the enstatite achondrites and no other major meteorite class (Lazzarin et al., 2004).

For asteroids with very low SC/OC, the radar echo is dominated by single backreflections from smooth surfaces, and in this case the Fresnel reflection coefficient R can be estimated with some confidence. For minerals that are plausible candi-

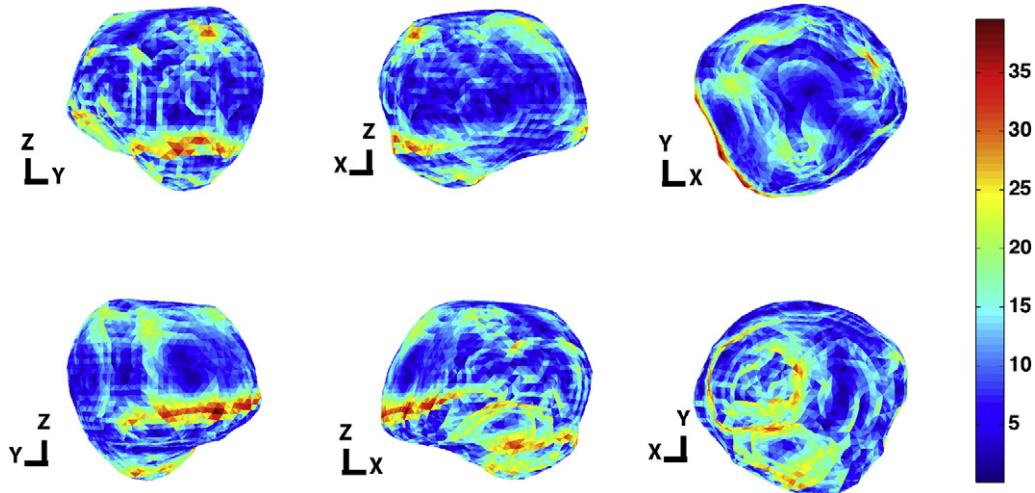


Fig. 6. WT24 model shaded for gravitational slope, assuming a uniform bulk density of 3 g cm^{-3} . For lower densities, the peaks near the north and south poles are outside the energetic Roche lobe, so loose material in these areas may escape the surface and go directly into orbit. Slope is given in degrees.

dates for asteroid surfaces, R depends most strongly on bulk density. Therefore, if the near surface is homogeneous, an estimate of R can be converted into an estimate of surface bulk density using approaches described most recently by Magri et al. (2001).

If SC/OC is high, then this logic breaks down: R cannot be estimated because multiple scattering and/or reflections from interfaces that are rough at scales near the wavelength dominate the echo. However, it may be possible to constrain the surface density in a relative sense, because the total-power (OC + SC) radar albedo is necessarily strongly related to the near-surface's average bulk density. WT24's total-power albedo ranks below values obtained for apparently metallic asteroids but above other NEAs, including objects whose global bulk densities have been measured by spacecraft: Eros ($2.67 \pm 0.03 \text{ g cm}^{-3}$; Yeomans et al., 2000) and Itokawa ($1.9 \pm 0.13 \text{ g cm}^{-3}$; Fujiwara et al., 2006). Therefore we expect that WT24's surface bulk density is most likely between 3 and 5 g cm^{-3} , but beyond this no strong constraints follow from our observations.

E-class asteroids are thought to have enstatite achondrite composition (Bus et al., 2002). Although some of those asteroids might contain high-density iron-bearing phases (Clark et al., 2004), there is no spectral evidence for high iron content minerals on WT24 (Lazzarin et al., 2004).

Solid enstatite achondrite has a bulk density of about 3 g cm^{-3} (Britt and Consolmagno, 2003). All this information suggests that WT24's surface and global bulk densities probably are close to 3 g cm^{-3} . Multiple-scattering configurations (along with a wide range of possible near-surface porosities) can conspire to give a wide range of total-power radar albedos, so with WT24 the radar properties do not constrain porosity. All we can say is that the near-surface structural complexity is severe. Our subjective physical intuition tells us that the most likely surface is dominated by cm-to-m-size rocks that have complex, jagged shapes.

4. Implications

4.1. Current structure and dynamics of WT24

Despite its extreme roughness at radar wavelengths, on scales of 10 m and larger the surface of WT24 is relatively subdued. Assuming a density of 3 g cm^{-3} , the average facet-scale gravitational slope (angle between the inward surface normal and the local acceleration vector) is 12° , and the maximum slope is 40° (Fig. 6). The equator and the depression near the south pole are the lowest potential regions (Fig. 7). While the necessary escape speed (for which a particle launched away from the surface at a given location on any trajectory is guaranteed to escape) varies between 19 and 33 cm s^{-1} , the sufficient escape speed (at which there is some escape trajectory from a given location) is between 0 and 13 cm s^{-1} . The zero in sufficient escape speed corresponds to the rotational Roche lobe intersecting the asteroid's surface near -70° latitude and 30° longitude—near the highest point of the potential. In this area, an object disturbed with minimal speed can in principle escape from the asteroid.

4.2. The evolution of WT24's spin state

The rotation states of near-Earth asteroids are not constant, being continuously subject to torques from radiation pressure and thermal re-radiation (the YORP effect), which are functions of the asteroid's orbit, current spin state, shape, and surface properties (Bottke et al., 2006). Using the method of Scheeres (2007) and Scheeres and Mirrahimi (2007), we have computed the spin-state evolution of WT24. We assumed that WT24 remains in a principle-axis rotation state, as it is now, and that the asteroid's thermal properties are constant over its surface. We averaged the incident solar energy over the orbit, and computed the torques on the asteroid as a function of its thermal properties and spin state. We have further assumed that the asteroid's orbit is constant, which limits the validity of our estimates to perhaps

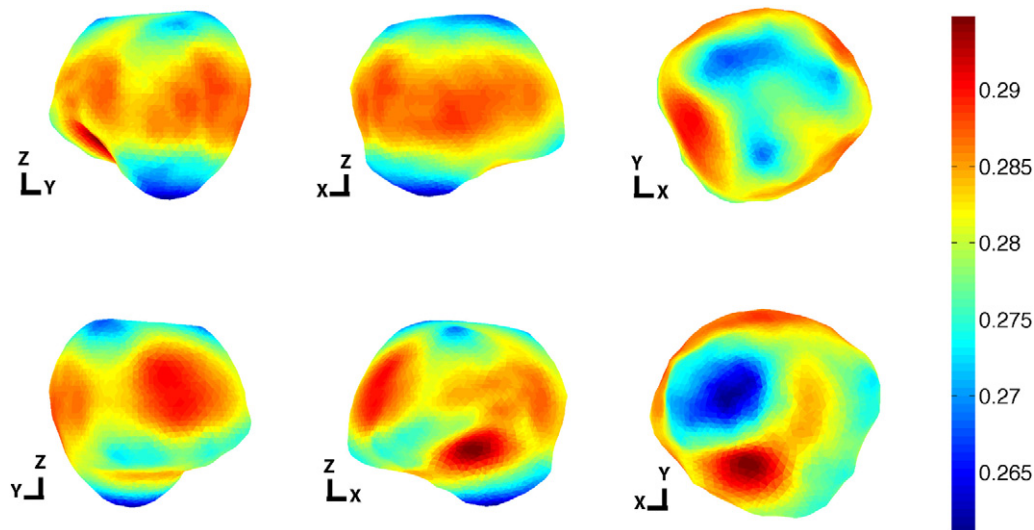


Fig. 7. Model shaded for potential, given in m s^{-1} acquired by an object falling from infinity to the surface. The red regions denote potential lows and the blue areas potential highs. Note the potential lows around the equator and in the south pole basin.

the last million years (NEODys, 2008). Over longer timescales changes in the asteroid's orbit will change the magnitude of the torques.

We find that for the thermal properties measured by Harris et al. (2007), WT24 is currently spinning down at an average rate of $2 \times 10^{-7} \text{ deg s}^{-1} \text{ yr}^{-1}$. At this rate the asteroid will be despun in approximately 150 kyr. If we extrapolate backwards in time at this current rate, we find that 75 kyr ago the asteroid had a period of 2.5 h, a rate that would place some regions of its surface at orbital velocity, suggesting that if the asteroid is composed of several monolithic components, these may have been in orbit about each other. If so, WT24 may have gone through a period of reconfiguration, as has been hypothesized for Itokawa (Fujiwara et al., 2006), which would modify its shape and change its YORP characteristics.

However, simply extrapolating the current deceleration rate forwards and backwards in time is not valid, because the obliquity of the asteroid is also changing, and hence so are the YORP torques. The obliquity changes are sensitive to the asteroid's thermal properties, in particular the average thermal lag angle—the angle between the sub-solar point and the highest temperature location. Using the Harris et al. (2007) estimate of WT24's thermal inertia and the Rubincam (1995) definition of the thermal lag angle in terms of thermal inertia and average equilibrium temperature, the average thermal lag angle of WT24 is between 1° and 10° . If the average thermal lag angle exceeds $\sim 6^\circ$, in the recent past WT24 was spinning at breakup with obliquity near 90° , and will continue to spin down. If the lag angle is low it was spinning *slower* in the past, with obliquity $\sim 180^\circ$, and will spin up in the future. An intermediate lag angle (close to 6°) can balance between these two cases. To determine the current thermal lag angle more precisely would require a thermal model incorporating the shape of the object, and would illuminate the spin-state history of the object.

If WT24 was once spinning at its breakup rate, the internal structure of the asteroid may be several pieces resting on each

other that were previously in mutual orbit. In this case, the asteroid's surface is too young to have three large craters, so the basins are either preexisting on the fragments, or more likely simply reflect the shape of the reaccumulated fragments.

5. Future observations

WT24 makes a 0.028 AU (11 lunar distance) Earth approach in December 2015. During this approach, the Yarkovsky perturbation to its trajectory may be marginally detectable if radar ranging is also obtained during 2012 (Vokrouhlicky et al., 2005). More importantly, the YORP perturbation predicted from our model corresponds to $\sim 600^\circ$ of rotation phase between 2001 and 2015, so it can be measured easily. For comparison, the recent measurement of the YORP torques on 54059 YORP, reported by Taylor et al. (2007), amounted to 250° of rotation phase. Even without additional radar observations, with sufficient lightcurve data it may be possible to detect variations in WT24's spin state well before 2015.

Supplementary material

The online version of this article contains additional supplementary material.

Please visit DOI: 10.1016/j.icarus.2008.01.020.

References

- Belskaya, I.N., Shevchenko, V.G., Kiselev, N.N., Krugly, Y.N., Shakhovskoy, N.M., Efimov, Y.S., Gaftonyuk, N.M., Cellino, A., Gil-Hutton, R., 2003. Opposition polarimetry and photometry of S- and E-type asteroids. *Icarus* 166, 276–284.
- Benner, L.A.M., 2008. Summary of asteroid radar detections, available online at http://echo.jpl.nasa.gov/~lance/asteroid_radar_properties.html.
- Benner, L.A.M., Ostro, S.J., Magri, C., Nolan, M.C., Howell, E.S., Giorgini, J.D., Margot, J.-L., Busch, M.W., Shepard, M.K., Taylor, P.A., Jurgens, R.F., 2008. Near-Earth asteroid surface roughness depends on compositional class. *Meteorit. Planet. Sci.*, submitted for publication.

- Bottke, W.F., Vokrouhlicky, D., Rubincam, D.P., Nesvorny, D., 2006. The Yarkovsky and YORP effects: Implications for asteroid dynamics. *Annu. Rev. Earth Planet. Sci.* 34, 157–191.
- Britt, D.T., Consolmagno, G.J., 2003. Stony meteorite porosities and densities: A review of the data through 2001. *Meteorit. Planet. Sci.* 38, 1161–1180.
- Bus, S.J., Villas, F., Barucci, M.A., 2002. Visible-wavelength spectroscopy of asteroids. In: *Asteroids III*. Univ. of Arizona Press, Tucson, AZ, pp. 169–182.
- Clark, B.E., Bus, S.J., Rivkin, A.S., McConnochie, T., Sanders, J., Shah, S., Hiroi, T., Shepard, M., 2004. E-type asteroid spectroscopy and compositional modeling. *J. Geophys. Res.* 109, E02001.
- Di Martino, M., and 17 colleagues, 2004. Results of the first Italian planetary radar experiment. *Planet. Space Sci.* 52, 325–330.
- Fujiwara, A., and 21 colleagues, 2006. The rubble-pile asteroid Itokawa as observed by Hayabusa. *Science* 312, 1330–1334.
- Harris, A.W., Mueller, M., Delbó, M., Bus, S.J., 2007. Physical characterization of the potentially hazardous high-albedo Asteroid (33342) 1998 WT24 from thermal-infrared observations. *Icarus* 188, 414–424.
- Kiselev, N.N., Rosenbush, V.K., Jockers, K., Velichko, F.P., Shakhovskoj, N.M., Efimov, Y.S., Lupishko, D.F., Rumyantsev, V.V., 2002. Polarimetry of near-Earth Asteroid 33342 (1998 WT24). In: Warmbein, B. (Ed.), *Proc. of the Conference: Asteroids, Comets, Meteors, ACM 2002*. ESA SP-500. ESA, Noordwijk, The Netherlands, pp. 887–890.
- Krugly, Y.N., Belskaya, I.N., Chiorny, V.G., Shevchenko, V.G., Gaftonyuk, N.M., 2002. CCD photometry of near-Earth asteroids in 2001. In: Warmbein, B. (Ed.), *Proc. of the Conference: Asteroids, Comets, Meteors, ACM 2002*. ESA SP-500. ESA, Noordwijk, The Netherlands, pp. 903–906.
- Lazzarin, M., Marchi, S., Barucci, M.A., Di Martino, M., Barbieri, C., 2004. Visible and near-infrared spectroscopic investigation of near-Earth objects at ESO: First results. *Icarus* 169, 373–384.
- Magri, C., Consolmagno, G.J., Ostro, S.J., Benner, L.A.M., Beeny, B.R., 2001. Radar constraints on asteroid regolith compositions using 433 Eros as ground truth. *Meteorit. Planet. Sci.* 36, 1697–1709.
- Magri, C., Ostro, S.J., Scheeres, D.J., Nolan, M.C., Giorgini, J.D., Benner, L.A.M., Margot, J.-L., 2007. Radar observations and a physical model of Asteroid 1580 Betulia. *Icarus* 186, 152–177.
- NEODys, 2008. Near-Earth objects—Dynamics, <http://newton.dm.unipi.it/cgi-bin/neoody/neoibo>.
- Pravec, P., 2007. Ondrejov Asteroid Photometry Project, available online at <http://www.asu.cas.cz/~ppravec/neo/htm>.
- Pravec, P., Harris, A.W., 2007. Binary asteroid population. I. Angular momentum content. *Icarus* 190, 250–259.
- Rubincam, D.P., 1995. Asteroid orbit evolution due to thermal lag. *J. Geophys. Res.* 100 (E1), 1585–1594.
- Scheeres, D.J., 2007. The dynamical evolution of uniformly rotating asteroids subject to YORP. *Icarus* 188, 430–450.
- Scheeres, D.J., Mirrahimi, S., 2007. Rotational dynamics of a Solar System body under solar radiation torques. *Celest. Mech. Dynam. Astron.*, submitted for publication.
- Taylor, P.A., and 11 colleagues, 2007. Spin rate of Asteroid (54509) 2000 PH5 increasing due to YORP effect. *Science* 316 (5822), 274–277.
- Veverka, J., and 13 colleagues, 1999. NEAR encounter with Asteroid 253 Mathilde: Overview. *Icarus* 140, 3–16.
- Veverka, J., and 32 colleagues, 2000. NEAR at Eros: Imaging and spectral results. *Science* 289, 2088–2097.
- Vokrouhlicky, D., Capek, D., Chesley, S.R., Ostro, S.J., 2005. Yarkovsky detection opportunities. I. Solitary asteroids. *Icarus* 173, 166–184.
- Yeomans, D.K., and 15 colleagues, 2000. Radio science results during the NEAR–Shoemaker spacecraft rendezvous with Eros. *Science* 289, 2085–2088.